

CHAPTER 4

Growth and Characterization of Cadmium Sulphide (CdS) Thin Films as a Buffer Layer

4. Growth and Characterization of Cadmium Sulphide (CdS) Thin Films as a Buffer Layer

Cadmium sulphide (CdS) is a group II–VI binary semiconductor compound, having an optical energy bandgap of 2.42 eV and wurtzite crystal structure. CdS becomes sublime at about 973 K and melts at about 2023 K under several atmospheric pressures. CdS in the thin film form has numerous applications such as, a buffer layer in copper indium diselenide (CIS) heterojunction based solar cells [73], transistors [108], photo detectors [109] and light emitting diodes [110]. Several deposition techniques have been used to fabricate CdS thin films, viz. electrodeposition [111] chemical bath deposition (CBD) [112] screen printing [113] and thermal evaporation [114]. Regardless of the deposition technique, the characterization of the deposited films and optimization of the deposition processes is still attracting researchers. Recent research interest in CdS thin films is largely sustained by its' application as a buffer layer material in polycrystalline thin film hetero-junction solar cells with CIS, as an absorber layer. The highest efficiency for thin film solar cells based on CIS absorber layer have been achieved using a CdS buffer layer deposited by a CBD process [22]. Although the CBD process for CdS deposition is very attractive owing to high solar conversion efficiency, for industrial production, an in-line vacuum deposition as, e.g., thermal evaporation is preferred [52]. In this chapter, investigation of structural, optical, and electrical properties of thermal evaporated CdS thin films is presented.

4.1 Utility of Buffer Layer in CIS Thin Film Solar Cell

The thin layer between the CIS absorber and zinc oxide layer (ZnO), a transparent conducting oxide (TCO), is known as a “buffer” or “window” layer. Although p-n junctions will form between TCO and p-type absorber layer, the quality of the junctions is improved considerably with the introduction of an intermediate buffer layer. The following functions are ascribed to buffer layers in thin-film CIS solar-cell junction.

- Buffer layer is usually highly-resistive, so it serves as an intermediate layer that can prevent shunting between the TCO and the absorber [115].
- Buffer layer can protect the absorber surface from damage by high-energy ions during the deposition of “window” layer using the sputtering process [116].
- Chemical constituents of buffer material passivate CIS surface defects and/or dope the CIS near-surface layer.
- Buffer layer affect the band structure. Specifically, they affect the band offsets and the electric field in the junction, and thus the current transport.

4.2 Criteria for Buffer Layer Selection

The criteria for selection of buffer layer follow directly from the previous section. A buffer material should be n-type, or possibly intrinsic (i-type) to make a good junction partner with a p-CIS absorber layer. Buffer with high resistivity are preferred to reduce the possibility of shunting of a junction. Matching the absorber and the buffer lattice constants, should also be considered when choosing a buffer. Poor matches may result in interfacial defects, which cause undesirable recombination of carriers. Technological feasibility of the incorporation of a buffer layer into the cell manufacturing process must also be considered.

The other major criterion in selection of a buffer material is its energy bandgap (E_g). E_g needs to be sufficiently wide so that as few photons as possible are absorbed in the buffer. This point is illustrated in figure 4.1 that shows the standardized solar spectrum, termed Air Mass 1.5 (AM1.5), in the units of photon current. The figure also shows the maximum photocurrent density (max- J_{sc}) that the light can generate in a solar cell as a function of the absorber layer bandgap E_g . For CIS absorber layer having $E_g = 1$ eV, the maximum J_{sc} is near to 46 mA/cm², whereas it is nearly 6 mA/cm² lower for 1.15 eV of CIGS. Note that despite the loss of current, one will still gain in efficiency by widening the absorber layer bandgap. The increase in efficiency should theoretically occur up to E_g (absorber) ~1.4 eV [117] due to increased V_{oc} .

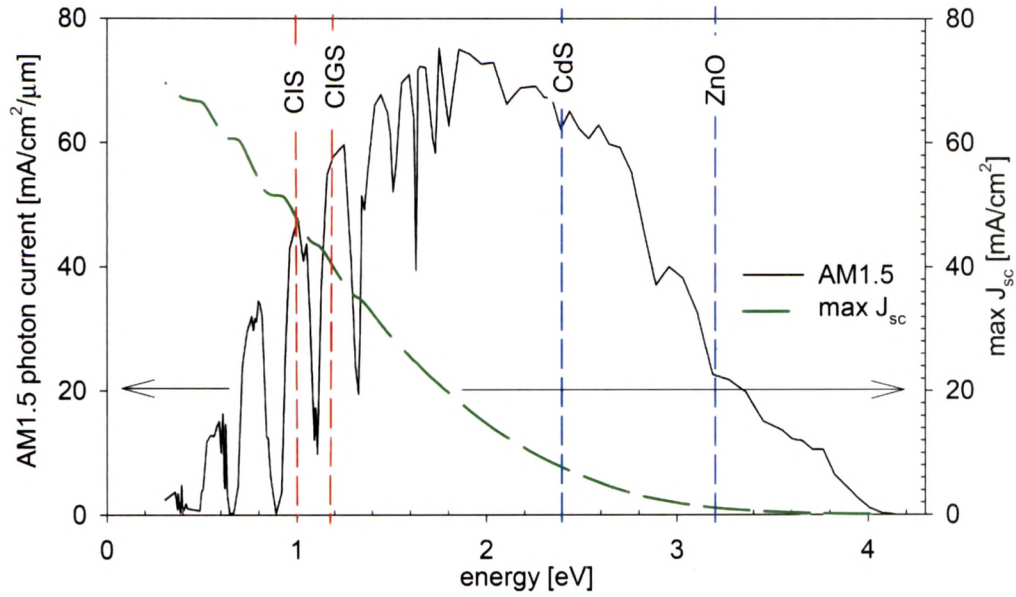


Figure 4.1: Standard AM1.5 solar spectrum; maximum attainable solar-cell short-circuit current density as a function of the absorber bandgap.

The max-J_{sc} calculations assume that all photons with $h\nu \geq E_g$ (absorber layer) are absorbed in the absorber and all minority carriers generated are collected at the junction. Before reaching the absorber, however, the incident light first passes through the front window layers. Photons with energies above the bandgaps of those layers will be absorbed there and the generated minority carriers will predominantly not be collected due to their low mobilities. As seen from figure 4.1 the bandgap of the Al doped zinc oxide (AZO) is $E_g = 3.2$ eV, which is nearly optimal in the sense that only a very small fraction of solar spectrum may be absorbed in ZnO layer resulting in photocurrent loss of less than 1 mA/cm^2 . CdS ($E_g = 2.4$ eV), however, can lower the photocurrent through absorption by up to $\sim 7 \text{ mA/cm}^2$. By making the CdS buffer layer thinner, part of the short-wavelength current loss can be recovered [118].

Another important buffer-material selection criterion is its electron affinity " χ " which will determine discontinuities in the energy bands at the buffer/absorber interfaces. There have been a number of various buffer materials and/or surface treatments incorporated in CIS based solar cells by various groups. Section 4.3 discusses the reported studies of various buffer material used in CIS based thin film solar cells.

4.3 Buffer Materials used in CIS based Thin Film Solar Cell

This section discusses different buffer layer material used in fabrication of CIS based thin-film solar cells by researchers.

4.3.1 Cadmium Sulphide (CdS)

Cadmium sulfide is a well-known material used as buffer layer in CIS based thin film solar cell. Record efficiency of up to 20.3 % [22] have been achieved in laboratory-scale CIS based solar cells with CdS buffer layer prepared by the chemical-bath deposition (CBD). Most CIS based solar cell modules use CdS as buffer layer.

The superior performance of CIS based solar cell with CdS buffer layer prepared by the CBD method is explored by K. Ramanathan et al. [119]. This group concluded that both sulfur and cadmium atoms favorably influence the surface or near-surface chemistry of CIS. Sulfur is suggested to passivate surface defects, and cadmium atoms are seen to diffuse into the near-surface region of the CIS film resulting, in additional defect passivation and/or n-type doping.

4.3.2 Zinc Oxide (ZnO), Cadmium Partial Electrolyte (Cd-PE) and Zinc Partial Electrolyte (Zn -PE)

CIS based solar cells without buffer layer, but with the intrinsic-ZnO layer had efficiencies that are typically considerably lower than those of CIS cells with CdS as buffer layer [120]. As discussed in the section 4.3.1, the work of Ramanathan et al. [119] showed that the CIS-surface treatment with cadmium or zinc partial electrolytes (Cd- PE or Zn- PE) increases the overall cell performance, but also smaller difference with the CdS-cells performance. Despite the increased short-wavelength currents in these cells due to the absence of a CdS layer; their V_{oc} values are typically somewhat reduced compared to CdS devices.

4.3.3 Zinc Oxy/Hydroxy Sulphide (ZnS(O,OH)) and Cadmium Zinc Sulphide (CdZnS)

The wide bandgap of zinc sulphide (ZnS) ($E_g = 3.8$ eV) makes this material an attractive buffer layer from the perspective of short-wavelength current. Solar cells made with nominal ZnS via the CBD method showed quite a respectable performance with record efficiency of 18.6 % for CIS based solar cell [121]. Secondary zinc oxide and hydroxide phases in CBD-

ZnS, however, are detected [122] in very large quantities in such cells. These compounds, which clearly alter properties of the thin film, have much lower E_c -offsets with CIS giving the discrepancy between the high performance of ZnS(O,OH)/CIS and a large ΔE_c for pure-ZnS/CIS. Additionally, ZnS can be unstable in an oxygen atmosphere and ZnO is formed when sufficient energy is provided [123].

Mixed CdZnS buffer materials have also been used for solar cell preparation. The reported efficiencies of $Cd_{1-x}Zn_xS$ /CIGS cell with buffer layer ($Cd_{1-x}Zn_xS$) deposited using the well known CBD technique have exceeded 19 % [124].

4.3.4 Zinc Selenide (ZnSe) and Zinc Indium Selenide ($ZnIn_2Se_4$)

ZnSe studies reported cell efficiencies as high as 14 %, and the study done at Hahn-Meitner showed the efficiency for ZnSe cells approaching that for the CdS reference cells made with the same absorber. The studies showed that ZnSe bandgap of $E_g = 2.67$ eV leads to photocurrents higher than those of CdS cells; however, obtained ZnSe-cell voltages are inferior. $ZnIn_2Se_4$ has relatively low bandgap of ~ 2.0 eV [115] for an ideal buffer-material candidate. Results from one of the two studies on $ZnIn_2Se_4$ are especially interesting. In that study, the buffer is deposited in the same vacuum cycle as (in-line with) the CIS based absorber layer, and the 15 % efficiencies are achieved. The reason for the good result is the close lattice-matching between the absorber and the buffer in this case, and the non-exposure of the absorber surface to air prior to the buffer deposition. Despite the low bandgap of $ZnIn_2Se_4$, its use in the in-line deposition process is thus demonstrated to be promising [125].

4.3.5 Indium Sulphide (In_2S_3)

The bandgap of crystalline β - In_2S_3 found in the literature is near 2.0 eV. The preparation of In_2S_3 via thermal evaporation, which is a “harder” deposition method, yielded cells with lower efficiencies than those for the CIS based solar cells with indium-sulfide buffers by atomic layer epitaxy (ALE), a “softer” method. According to the reports on cells with 1.8 eV, In_2S_3 buffers their efficiencies reached as high as 14.8 % [126]. Such cells have low photocurrents due to the low buffer bandgap.

4.4 Why CdS?

The theoretical efficiency of CIS based solar cell devices is around 28 % [66]. The best efficiency recently reported using CdS as buffer layer is 20.3 % [22], which makes these devices an interesting candidate for low cost solar energy conversion technology. A variety of buffer layer materials is investigated by researchers other than CdS as discussed in the section 4.3, but none have yet matched its performance [127], probably due to lattice parameter that matches well with that of the CIS layer (lattice mismatch around 1.2 %) [128].

4.5 CdS Thin Film Deposition using Thermal Evaporation Technique

CBD is the most commonly used technique to fabricate CdS films for CIS and CdTe based thin film solar cells with high efficiency [22, 129]. Thermal evaporation technique of CdS thin film deposition has potential to replace CBD technique but lower conversion efficiency achieved with CdS buffer layers as compared to CBD CdS thin film is the major concern [52]. Despite the fact that evaporated CdS thin films has been investigated from the point of view as a heterojunction partner to the absorber layer in solar cells there are many issues that still to be understood particularly the interface study of CIS/CdS. The Junction formation at the interface largely depends on quality of CdS thin films. Structural, morphological, optical and electrical properties of CdS thin films influence the junction operation. Therefore, optimization of growth condition of thermal evaporated CdS thin film is a prime concern.

In this work, CdS powder (99.995 %) obtained from Sigma-Aldrich (U.S.A.) is used to deposit thin films of CdS of size 1 cm × 1 cm onto organically cleaned sodalime glass substrates held at different temperatures ranging from 323 K-473 K using thermal evaporation technique. The rate of deposition and thickness of CdS films as measured using quartz crystal thickness monitor (Hind Hi Vac. DTM -101) are 0.1-0.2 nm/s and 30 nm-150 nm respectively. The substrate temperature is measured using chromel-alumel thermocouple kept in good thermal contact with the substrate. We have optimized deposition parameters of CdS layer and the optimized parameter of CdS thin film is used to prepare heterojunction with CIS layer.

4.6 Characterization of CdS Thin Films Deposited using Thermal Evaporation Technique

The structural characterization of CdS thin films deposited at different T_s are carried out using an x-ray diffractometer (Shimadzu Lab X 6000) in 2θ range 20° - 70° at a scan rate $0.05^\circ \text{ s}^{-1}$ with Cu K_α ($\lambda = 0.154 \text{ nm}$) radiation source and transmission electron microscope (TEM) (JEM-2100, JEOL make). The surface and chemical composition analysis of CdS thin films deposited at different T_s are carried out using scanning electron microscope (JEOL, JSM-5610LV) equipped with energy dispersive analysis of x-rays (EDAX) facility. The optical transmittance measurements are carried out in the wavelength range 320 nm-900 nm using the monochromator CM 110, photo detector 816-SL type (Newport) and lock-in amplifier SR-530. For the electrical measurements, four small indium contacts are deposited at room temperature on the surface of CdS films, which are arranged symmetrically at four corners. The electrical characterizations of CdS thin films deposited at different T_s are carried out using conventional Hall effect measurements at room temperature under normal light condition using Keithley 614 programmable electrometer and Keithley 181 nano-voltmeter.

4.6.1 Structural Characterization

The structural characterizations of CdS thin films having thickness of 150 nm deposited at different T_s have been investigated by x-ray diffraction (XRD) technique using Cu K_α radiation. As is well known, CdS can exist in two crystalline modifications: the hexagonal (wurtzite) phase and the cubic (zincblende) phase. For solar cell application, hexagonal CdS films are preferable due to its excellent stability [130]. XRD curves of CdS films deposited at different T_s is shown in figure 4.2.

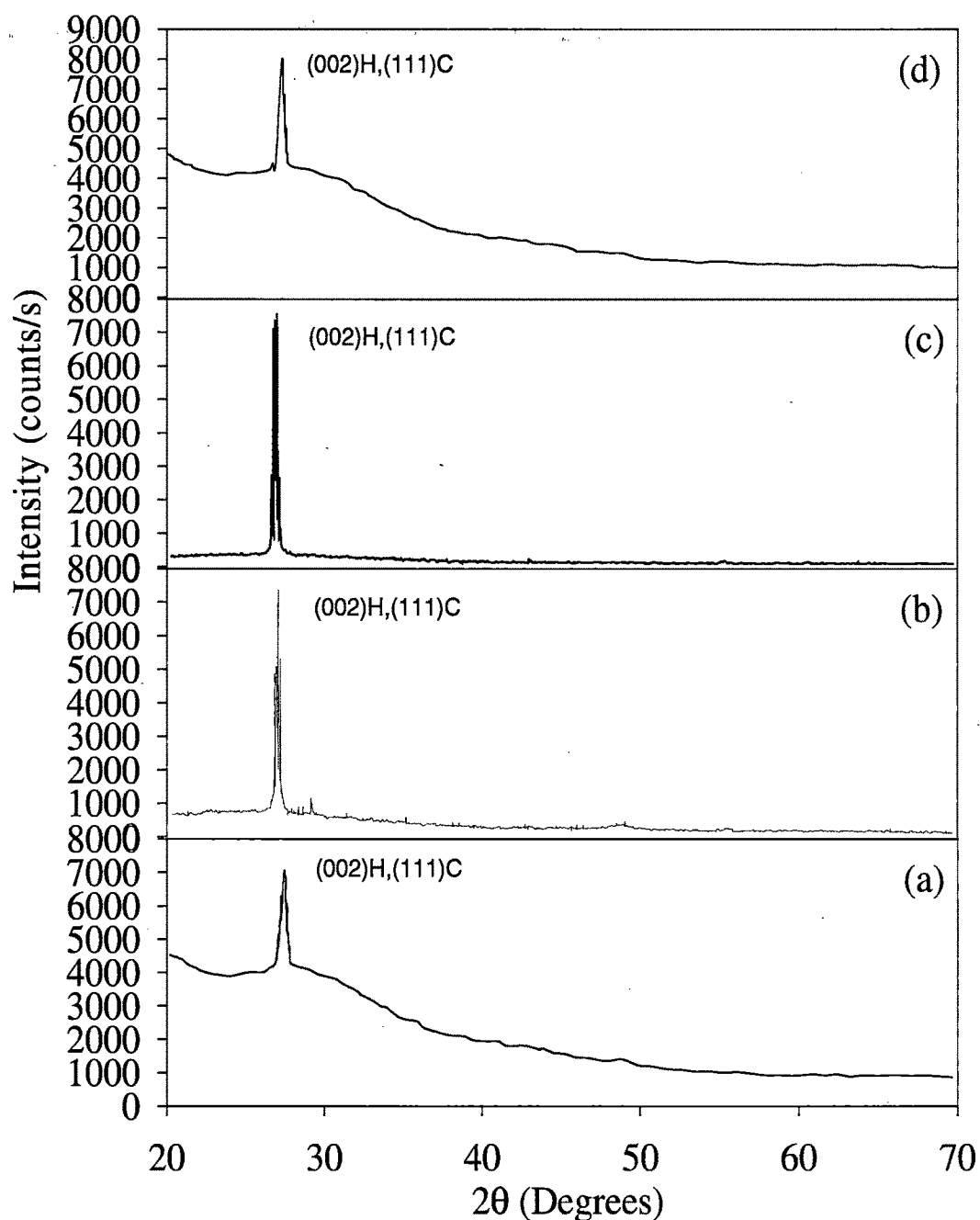


Figure 4.2: X-ray diffractograms of the CdS thin films prepared at different substrate temperatures: (a) $T_s = 323$ K, (b) $T_s = 373$ K, (c) $T_s = 423$ K, (d) $T_s = 473$ K.

All films showed a predominant single peak at $2\theta = 26.7^\circ$ which can be assigned to the (002) plane of hexagonal or the (111) plane of cubic CdS. This preferred orientation of CdS films is due to the controlled nucleation process associated with the low deposition rate. XRD analysis of CdS thin films deposited at different T_s revealed that all films had preferred orientation of grains corresponding to (002) diffraction plane of hexagonal structure or (111) reflections of cubic structure as shown in figure 4.3. Therefore, a straightforward structural

characterization of the as-deposited CdS film using XRD is difficult. For solar cell application, hexagonal CdS films are preferable due to its excellent stability [130]. So, to confirm the exact orientation of grains, the structural analysis of film deposited at 373 K is detected with TEM. The thickness of the film for TEM study is 40 nm. This enabled the films transparent to the electron beam. Sample for TEM study can be peeled off from the glass substrate using dilute hydrofluoric acid and set onto copper grid. TEM image with typical selected area diffraction (SAD) is shown in figure 4.3.

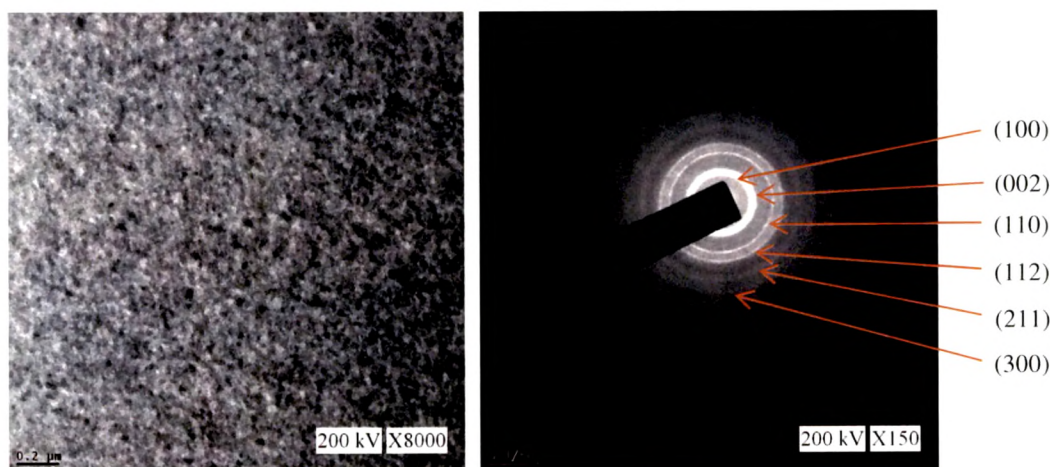


Figure 4.3: TEM and SAD image of CdS film deposited at 373 K.

The SAD pattern contains sharp rings expected for polycrystalline films. The diameter of rings (D_{hkl}) in the SAD pattern is measured using the formula $d_{hkl} = 2\lambda L/D_{hkl}$. Here, L is the camera length and λ is the wavelength of the electron beam calculated from accelerating potential. The calculated d values corresponds to three characteristic major intensity peaks (002), (110) and (112) matched well with those of the JCPDS data card 41-1049 of hexagonal α - CdS reflections. No cubic phase, complex of cubic and hexagonal or secondary phase is observed. The very prominent bright ring seen in SAD pattern due to the (002) plane indicates the preferred orientation along that direction. All the obtained (hkl) indices of the diffracted rings matched well with those of the JCPDS 41-1049 data [131] for hexagonal phase.

The mean size of the crystallites in CdS thin films deposited at different substrate temperatures are calculated from the (002) x-ray diffraction peak broadening using the well-known Scherer's formula after the correction for the instrumental spectral broadening. The peak position of (002) plane and FWHM of the (002) peak, along with the calculated values of the crystallite size, for films grown at different T_s are shown in table 4.1. The increase in

the crystallite size would result from the enhancement of the film surface atomic mobility with increasing T_s which enables the thermodynamically favored grains to grow.

Table 4.1: The position of (002) peak, full width at half maximum (FWHM) and crystallite size of CdS thin films grown at different T_s .

Substrate Temp. T_s K	Position of (002) peak (Degrees)	FWHM (Degrees)	Crystallite size d (nm)
323	27.31	0.4390	18
373	27.05	0.1732	47
423	27.03	0.1732	50
473	27.14	0.2770	29

4.6.2 Morphological Studies

The as-deposited films are smooth, optically transparent, adherent and light-yellow in color. The surface morphologies of the CdS films deposited at different T_s is studied using scanning electron microscope (SEM). Figure 4.4 shows SEM images of CdS films deposited at different substrate temperatures. No pinholes or surface defects are observed in SEM images of CdS films deposited at different T_s . The appearance of cracks in CdS film deposited at 373 K may be due to high tensile stress in the film. A similar observation has also been reported by other workers for their CdS thin films [132] deposited using CBD method.

4.6.3 Compositional Characterization

The composition of CdS thin films used as buffer layer is a topic of important since many cell properties are influenced by deviations from stoichiometry of buffer layer. The compositional analysis of the CdS thin films deposited at different substrate temperatures is carried out using EDAX measurements. Figure 4.5 shows the energy dispersive analysis of x-rays (EDAX) spectrographs of CdS thin films deposited at different substrate temperatures. Table 4.2 shows at. wt. % of CdS thin films of 150 nm deposited at different T_s . The ratio of Cd to S approaches to 1.0 as the T_s approaches to 400 K. However, all the films have some Cd excess over S.

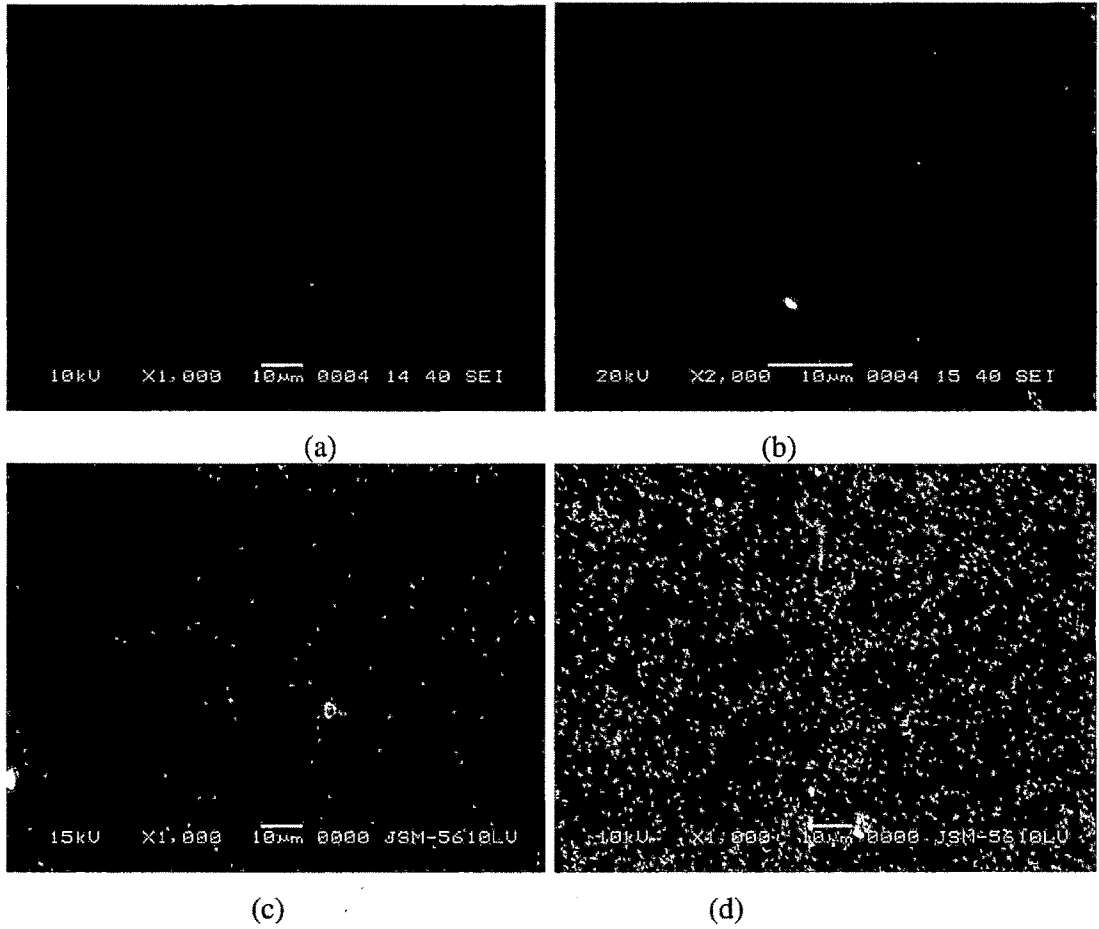
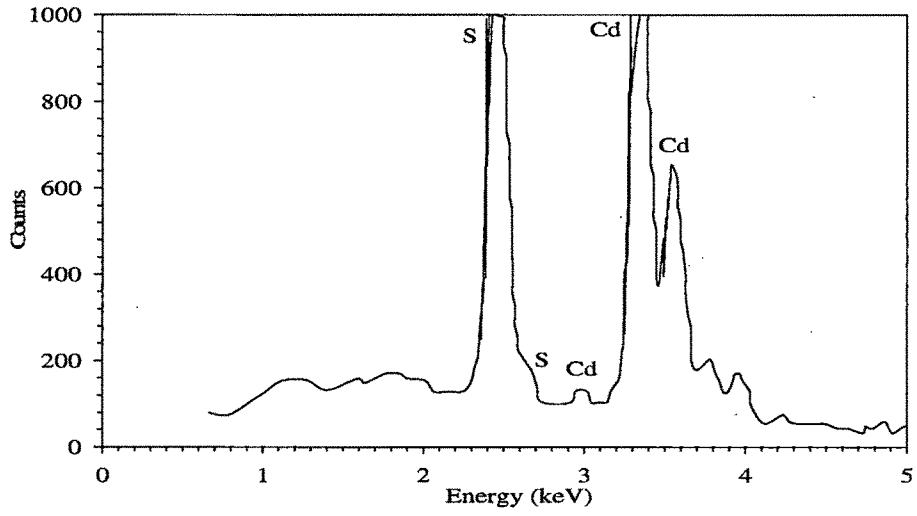


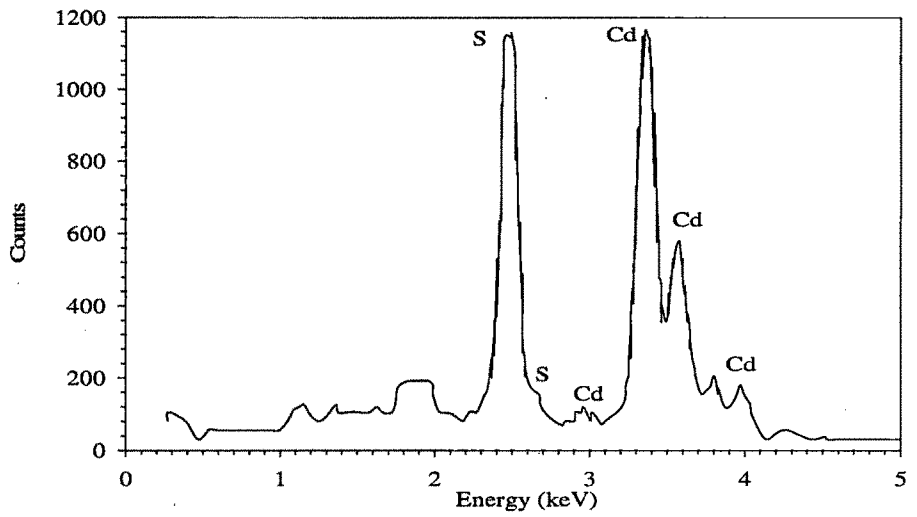
Figure 4.4: SEM micrographs of CdS films deposited at (a) $T_s = 323$ K, (b) $T_s = 373$ K, (c) $T_s = 423$ K and (d) $T_s = 473$ K.

Table 4.2: EDAX analysis of CdS thin films grown at different substrate temperatures.

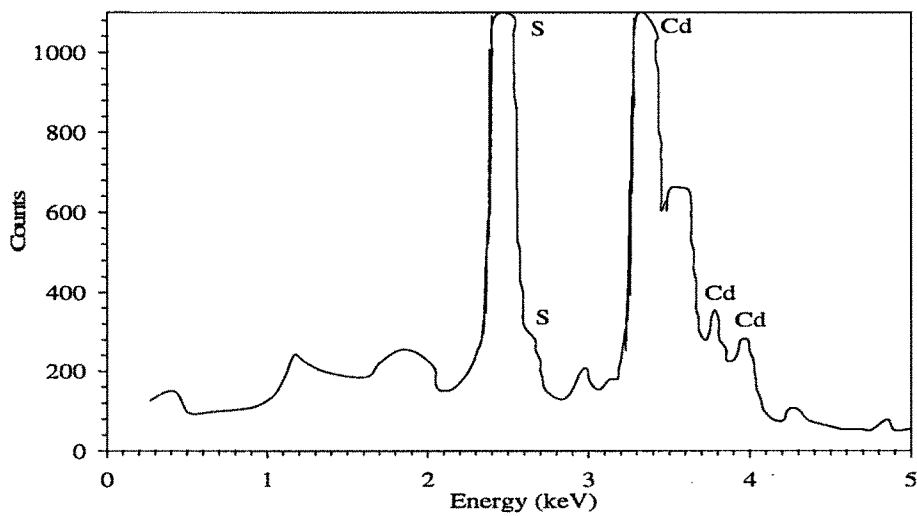
Substrate Temperature T_s (K)	Elemental composition (at. wt. %)		Ratio Cd/S
	Cd	S	
323	49.09	50.91	0.96
373	49.33	50.67	0.97
423	49.93	50.07	0.99



(a)



(b)



(c)

Figure 4.5: EDAX spectrograph of CdS thin films (a) $T_s = 323$ K, (b) $T_s = 373$ K, (c) $T_s = 423$ K.

4.6.4 Optical Characterization

The transmittance spectra of CdS thin films deposited at different T_s , is shown in the figure 4.6. It can be found that the thermally evaporated CdS films present high transmission (70-90 %) and low absorbance in the visible region. The absorption coefficient (α) is calculated from the experimental measured values of transmittance T using the relation described in section 2.2.6. Values of absorption coefficient of CdS thin films deposited at different substrate temperatures are used to calculate energy bandgap. The plots of $(\alpha h\nu)^2$ with photon energy $h\nu$ for films grown at different substrate temperatures is shown in figure 4.7. Extrapolation of the linear portion of the curve to $(\alpha h\nu)^2 = 0$ gives the bandgap energy which is in the range 2.40-2.45 eV which is in good agreement with the bandgap values by many earlier works [133, 134]. At $T_s = 423$ K, the energy bandgap value for CdS thin decreases with increase of substrate temperature.

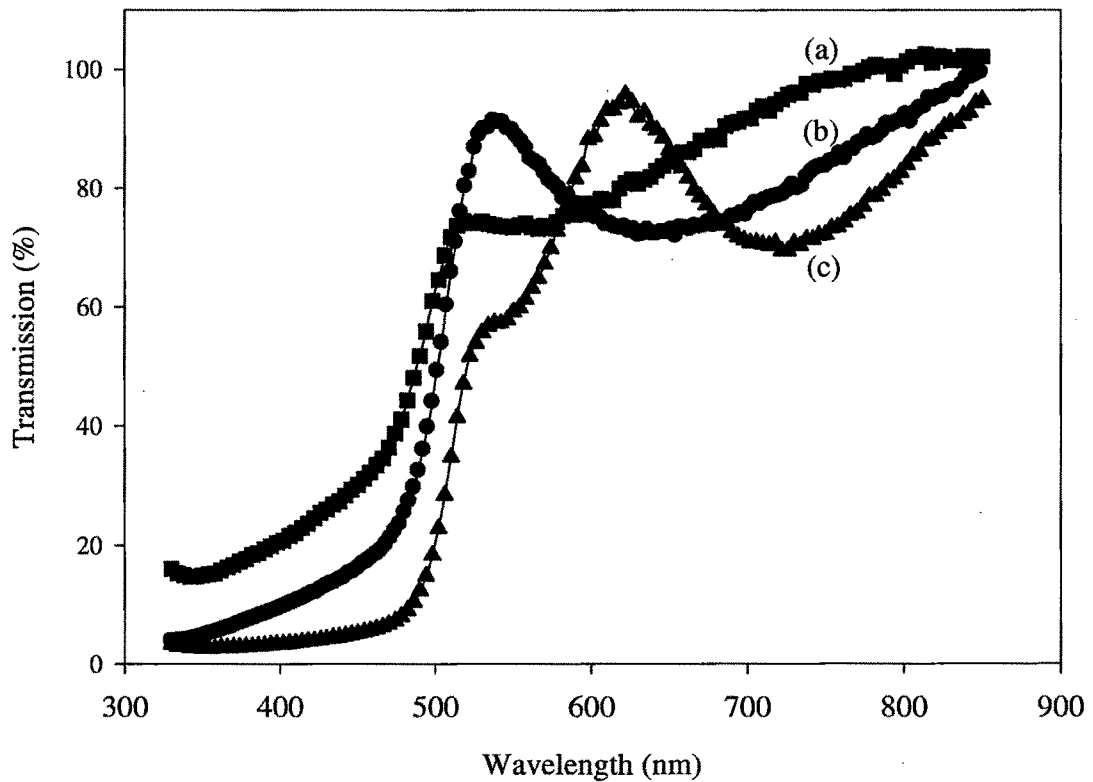


Figure 4.6: Transmission spectra of CdS thin films (a) $T_s = 323$ K, (b) $T_s = 373$ K, (c) $T_s = 423$ K.

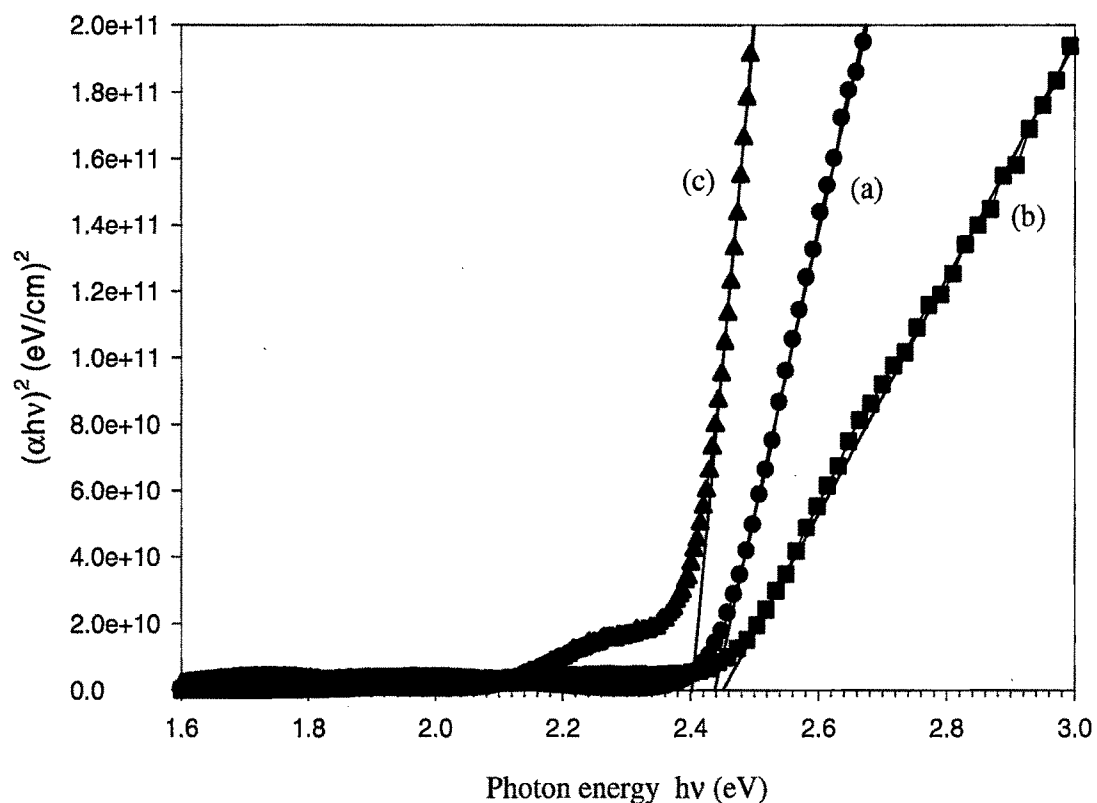


Figure 4.7: Plots of $(\alpha hv)^2$ vs (hv) for CdS thin films (a) $T_s = 323$ K, (b) $T_s = 373$ K, (c) $T_s = 423$ K.

The decrease in energy bandgap at $T_s = 423$ K is due to the influence of various factors such as crystallite size, structural parameters, deviation from stoichiometry of the film etc. However, we have observed that crystallite size has a direct dependence on substrate temperature. Hence we consider that the observed decrease in energy bandgap at $T_s = 423$ K is due to increase in crystallite size and decrease in strain and dislocation density. CdS thin film deposited at 373 K has energy bandgap value of 2.45 eV, optimum for its use as a buffer layer in solar cell. Thickness dependence of energy bandgap for film deposited at 373 K is also investigated to optimize film thickness for its use as a buffer layer in thin film solar cell. Figure 4.8 shows that in the thickness range (30-150 nm) that we have studied the energy bandgap increases as thickness of the film increases. The range of optical bandgap is found to lie between 2.33-2.44 eV with increasing film thickness and approaches value of single crystalline CdS (2.42 eV) [66].

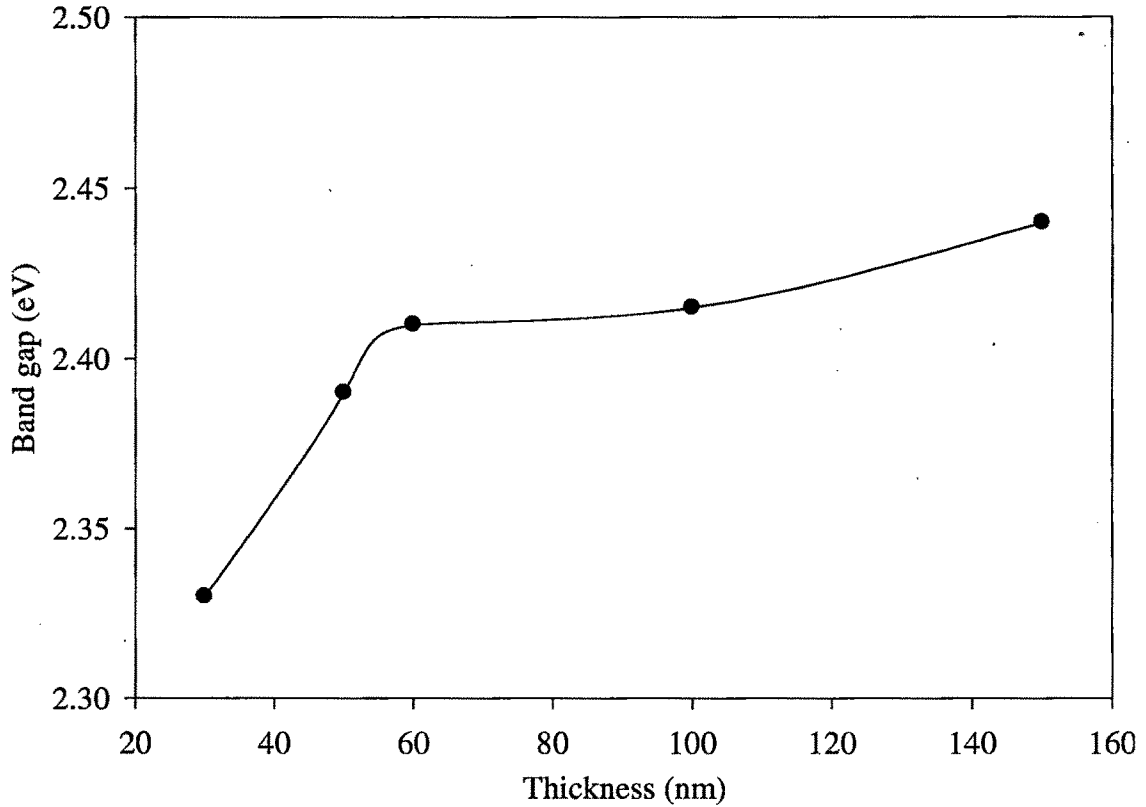


Figure 4.8: Dependence of energy bandgap of CdS thin films on thickness.

4.6.5 Electrical Characterization

The resistivity and mobility value of CdS films deposited at different substrate temperature measured at room temperature is shown in the figure 4.9. The resistivity value range from $1.3 \times 10^4 \Omega \text{ cm}$ to $7.9 \times 10^4 \Omega \text{ cm}$ for films with thickness of 150 nm deposited at different T_s . The data show that the resistivity increased as the T_s increased upto 423 K and then decreases with increase of T_s . The high resistivity of CdS films resulted from the good stoichiometry and the lack of defects. The order of resistivity in the present work is in the range of $\sim 10^4 \Omega \text{ cm}$, which is suitable for application of CdS films as a buffer layer in thin film solar cells based on CIS. These results of resistivity are quite similar to those obtained by Su and Choy [135] using spray deposition and Ashour et al. by modified thermal evaporation source [136]. The electron mobility value of CdS films increase with T_s , have a maximum at 423 K T_s and decrease thereafter. Similar behavior is observed by Kazamerski et al. [137] for CdS films deposited using thermal evaporation method.

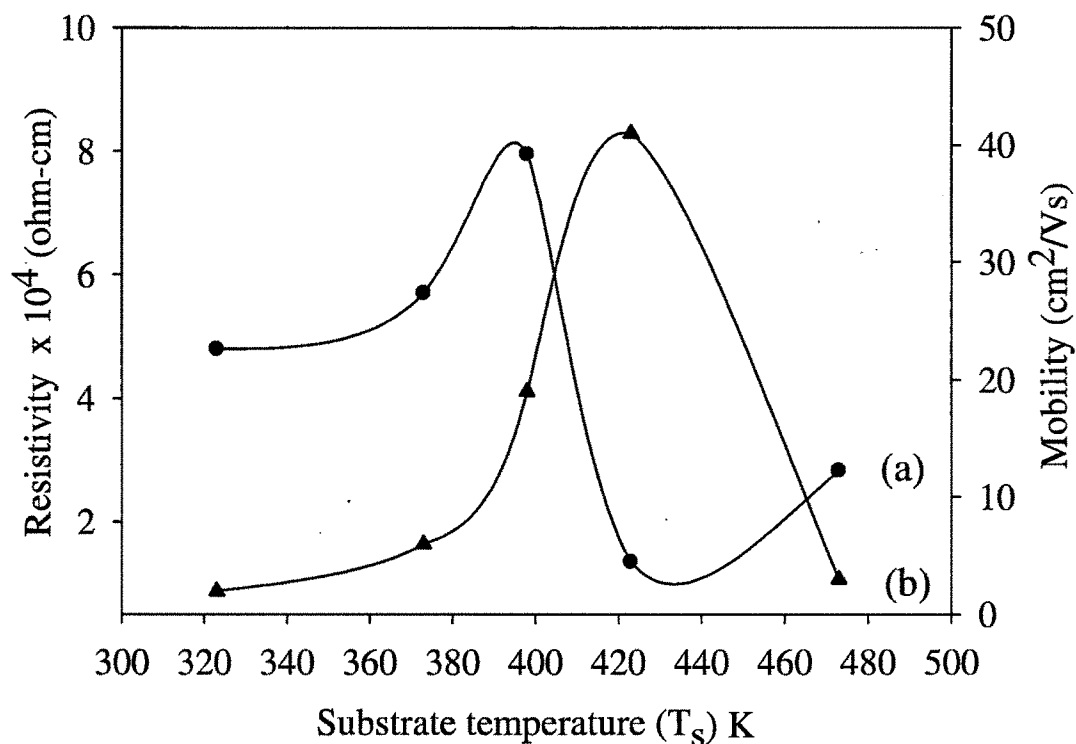


Figure 4.9: Variation of a) Resistivity and b) mobility of CdS thin films deposited at different substrate temperatures.

The decrease in resistivity with the increase in substrate temperature can be explained using Petritz's barrier model [106]. According to which at low temperatures, the crystallites do not grow sufficiently large while at higher substrate temperature large crystallite sizes are obtained which ultimately decrease the intercrystalline barrier, therefore have to cross comparatively narrow intercrystalline barriers and this result in decrease of resistivity.

Conclusions

CdS thin films are deposited on glass substrates held at different temperatures using thermal evaporation technique showed good optical properties and adhered well to the substrates. XRD and TEM pattern of these films indicated that the deposited CdS films contain hexagonal (wurtzite) structure. The crystallite size is found to be 18-50 nm for films deposited at different T_s . Analysis of SEM images suggests that T_s had obvious affection for the morphology. The increase of T_s improves the surface morphology of the CdS films. The optical and electrical investigations prove that CdS film deposited at 373 K have high transparency, energy bandgap of 2.45 eV and higher value of resistivity suitable for its' application as a buffer layer in CIS based thin film solar cell.